Chinese Journal of Chemical Engineering 95 (2026) 217–225

Contents lists available at ScienceDirect

Chinese Journal of Chemical Engineering

journal homepage: www.elsevier.com/locate/CJChE

Full Length Article

Computational modeling of nanoplastic particles for polymer-binding peptide interactions at atomistic resolution

Yingqian Ren [1], Mingyu Wang [1], Jipeng Li [2,*], Xingqing Xiao [1,*]

[1] School of Chemistry and Chemical Engineering, Hainan University, Haikou 570228, China
[2] School of Marine Sciences, Hainan University, Haikou 570228, China

ARTICLE INFO

Article history:
Received 3 November 2025
Received in revised form
27 January 2026
Accepted 28 January 2026
Available online 15 April 2026

Keywords:
Peptide–polymer interactions
Computational modeling and simulation
Molecular recognition
Thermodynamics properties

ABSTRACT

Investigating the specific interactions between polymers and functional peptides allows for the rational discovery of polymer-binding peptides. These peptides can be applied to capture dispersed and dissolved nanoplastic particles in water. Molecular dynamics (MD) simulations require that the force field accurately describe the polymers' physicochemical properties. This study utilized the generalized AMBER force field 2 (GAFF2) to simulate the folding conformations of three common polymer chains — polyethylene (PE), polypropylene (PP), and polystyrene (PS) — in an aqueous solution. The power law relationship between the radius of gyration and chain length was calculated to compare theoretical predictions. Additionally, the density and heat capacity of polymer melts were simulated and compared with experimental measurements. The simulation results confirmed the reliability of the GAFF2 in describing polymers. Subsequently, we examined molecular interactions between nanoplastic particles and polymer-binding peptides in the explicit-solvent MD simulations. Binding free energy calculations revealed that the HNKSSPLTAALP peptide exhibited the strong affinity for PE particles, followed by the TSDIKSRSPHHR peptide for PP particles, and the HWGMWSY peptide for PS particles. van der Waals interactions are essential for the specific recognition of molecules between peptides and polymers.
© 2026 The Chemical Industry and Engineering Society of China, and Chemical Industry Press Co., Ltd. All rights are reserved, including those for text and data mining, AI training, and similar technologies.

1. Introduction

Microplastic and nanoplastic pollution has emerged as a significant environmental concern, attracting broad attention over the past two decades [1]. These pollutants are present in the air, water, and soil [2], with millions of tons of microplastic waste estimated to be found in the environment [3]. In contrast, there are currently no reliable estimates for nanoplastic waste, as capturing and identifying nanoplastics remains a challenge [4]. The health risks associated with this pollution — particularly nanoplastics — are still under investigation but may become more pronounced as plastic waste continues to accumulate [5]. While there is an urgent need to remove microplastic and nanoplastic waste from the environment, an efficient, large-scale removal technique has yet to be developed. Peptides have attracted interest as effective bio-recognition elements for biomacromolecules, as they can be easily used to functionalize material surfaces for various applications [6,7]. For instance, polymer-binding peptides [8,9] could be incorporated into membranes or attached to mobile particles to capture plastic waste in water. So far, the discovery of functional peptides still relies on phage display library screening. However, this method does not always yield high-affinity peptides due to inherent library biases and the presence of parasitic sequences [10].

Building on our previously developed peptide binding design (PepBD) algorithm [11–14], we are now extending its application to computationally discover peptide-based binders with high affinity for specific polymers. This effort is driven by a motivation to gain a deeper molecular-level understanding of peptide–polymer interactions, which are ubiquitous in nature. Examples include neurotransmitters such as enkephalins involved in signal transduction [15], as well as neuromodulators such as oxytocin involved in the action of hormones [16]. Accurate characterization of how proteins interact with polymers is crucial for exploring their binding mechanism at nanoscale interfaces [17], yet experimental methods cannot fully capture these details. Therefore, multiscale computational approaches have been proposed to study the fundamental interactions associated with biomolecules and macromolecules, aiming to reproduce structure-related properties

* Corresponding authors.
E-mail addresses: lijipeng@hainanu.edu.cn (J. Li), xqxiao@hainanu.edu.cn (X. Xiao).

https://doi.org/10.1016/j.cjche.2026.01.026
1004-9541/© 2026 The Chemical Industry and Engineering Society of China, and Chemical Industry Press Co., Ltd. All rights are reserved, including those for text and data mining, AI training, and similar technologies.

such as the lower critical solution temperature (LCST) [18] and the order-disorder transition (ODT) [19]. It is important to recognize that the reliability of computational modeling strongly depends on the selection of force fields capable of precisely representing the physical and chemical properties of both biomolecules and macromolecules. The generalized AMBER force field 2 (GAFF2) is favored for its compatibility with available parameter sets for both proteins and polymers, as well as its validation against experimental data.

Evaluation of polymer–peptide binding requires molecular dynamics (MD) simulations at atomistic resolution. While previous computational studies on protein adhesion to polymers or on protein–polymer conjugates have often relied on coarse-grained models [20], these approaches are inadequate for polymer-binding peptide design because they omit critical structural details of both amino acids and polymer monomers. Atomistic MD simulations typically utilize general force fields such as CHARMM [21], the generalized Amber force field (GAFF) [22], or OPLS-AA [23] to model polymers. However, there has been little evaluation of how accurately these force fields simulate common polymers like polyethylene (PE), polypropylene (PP), and polystyrene (PS). GAFF2, an improved version of the original GAFF, better accounts for the experimental properties of organic compounds [24]. For example, GAFF2 includes explicit torsional barriers (*e.g.*, for O–C–C–O and N–C–N–C) that were absent from GAFF [25]. Additionally, its updated van der Waals (VDW) parameters accurately reproduce experimental liquid density, heat of vaporization, *etc*. [26] Therefore, this study aims to assess the ability of the GAFF2 to reproduce experimentally determined polymer properties before employing it in peptide binding simulations.

The paper is organized as follows. Section 2 details the methods employed for conducting MD simulations. Section 3 assesses the performance of GAFF2 in simulating PE, PP, and PS polymers, and also presents the outcomes of peptide–polymer binding simulations. Section 4 discusses the findings and explores their implications for the design of polymer-binding peptides.

2. Methods and Modeling

2.1. Quantum mechanics calculations and restrained electrostatic surface potential charge fitting

Partial atomic charges for PE, PP, and PS monomers are not available in AMBER force fields. To address this, quantum mechanical (QM) calculations were conducted using Gaussian 16 software to determine the partial atomic charges. A two-stage restrained electrostatic surface potential (RESP) charge-fitting protocol [27] was employed, with the total charge of each monomer constrained to zero. First, the monomer geometry was optimized at the HF/6-31G(d) level, followed by calculation of the electrostatic surface potential (ESP) using the B3LYP/6-31G(d) basis set. In the first stage of the RESP charge-fitting protocol, a least-squares fit was used to yield partial charges to reproduce the ESP. In the second stage, the partial charges of hydrogen atoms in the methyl and methylene groups were set to be equal.

2.2. Simulation of polymer folding in water and radius of gyration calculations

The Antechamber tool was used to create topology and coordinate files for the monomers of three polymers: PE, PP, and PS. While the GAFF2 parameters were applied to all monomers except for partial charges. For each polymer, library files were generated by producing a pair of coordinate and topology files, which were then converted into mol2 format. These library files facilitated the construction of initial linear conformations for PE, PP, and PS polymer chains of varying lengths using the XLEAP module (Fig. S1, in Supplementary Material). Simulations were performed using the AMBER22 package on six distinct chain lengths — 30, 50, 100, 150, 200, and 250 units — referred to as “PE30”, “PE50”, …, “PP100”, “PP150”, …, “PS200”, and “PS250” for brevity.

As illustrated in Fig. S1, a very large periodic cubic box would be required to accommodate the linear polymer chains for folding studies using explicit-solvent atomistic MD simulations. Therefore, we initially performed implicit-solvent atomistic MD simulations for 10°ns at 500 K to partially relax the linear polymer chains. The elevated temperature was chosen to prevent the polymer conformations from being trapped in local minimum. During the implicit-solvent MD simulations, the SHAKE algorithm was used to constrain bonds involving hydrogen atoms, and a Langevin thermostat maintained the system at the desired temperature. No cut-off distance was applied when computing VDW and electrostatic interactions. The resulting partially folded polymer chains were then solvated within a 1.5 nm buffer of TIP3P water, allowing for complete relaxation during subsequent explicit-solvent annealing simulations. These simulations were conducted in the isothermal–isobaric (NPT) ensemble, with the Langevin thermostat controlling the temperature and the Berendsen barostat maintaining the pressure at 100 kPa with a time step of 0.5 ps. The SHAKE algorithm and Langevin thermostat were again employed. Long-range electrostatic interactions were calculated using the particle mesh Ewald method, while long-range VDW interactions were cut off at 0.8 nm. The annealing process involved gradually reducing the temperature from 400 K to 300 K in 5 K increments every 5 ns, resulting in a total annealing MD simulation time of 100 ns.

The last 5°ns simulation trajectory was utilized to analyze the folded conformation of the polymer chain at equilibration. To assess this, the average radius of gyration (R_g) was calculated based on the backbone carbon atoms C1 and C2, which is defined as $R_g = \sqrt{\frac{1}{N}\sum_{k=1}^{N}(\boldsymbol{r}_k - \boldsymbol{r}_c)^2}$, where N represents the length of the polymer chain, $\boldsymbol{r}_k$ is the position of the k_{th} heavy atom (either C1 or C2), and $\boldsymbol{r}_c$ denotes the center of mass of the polymer chain.

2.3. Simulation details for studying the physicochemical properties of pure polymers

The capability of the GAFF2 to capture polymer properties was further assessed by measuring the density of the polymers. Atomistic simulations were performed using ten 150-mer polymer chains in the NPT ensemble at 300 K. Rather than starting from initial linear conformations, the folded conformations obtained from R_g calculations were utilized. Periodic cubic boxes were set up to accommodate all ten polymer chains. The pressure increased gradually, beginning at 10 kPa. An NPT simulation was run for 5°ns at each pressure increment, which was raised by 10 kPa after each simulation, continuing this process until reaching 100 kPa for a total of 50°ns of simulation time. Equilibration was confirmed by monitoring both pressure and energy throughout each NPT simulation. The density at 100 kPa was then calculated based on the size of simulation box at equilibrium and the total system mass. Noted that no solvent was included in these simulations, so the measured density reflects that of a polymer melt.

The specific heats of the polymers were also measured. The specific heat capacity remains approximately constant between 300 K and 320 K, allowing its calculation from the change in enthalpy (ΔQ) with respect to temperature (ΔT) at constant pressure, using the equation $C_p = \Delta Q/\Delta T$ [28]. To evaluate polymer enthalpy at different temperatures, MD simulations were carried

out in the NPT ensemble using the folded 150-mer polymer structures. All simulations were conducted at 100 kPa, with the temperature varied from 300 K to 320 K in 2 K increments. For each temperature, a 5°ns production simulation ensured the system reached equilibrium. The C_p of the pure polymers was obtained from the slope of the plot of average enthalpy *versus* temperature. Enthalpy was calculated as the sum of internal energy, VDW energy, and electrostatic energy over all atoms in the system. No solvent was present in the simulations, so the measured C_p corresponds to that of a polymer melt.

For each polymer system, four independent production simulations were conducted using the AMBER22 package to determine their density and heat capacity in the molten state.

2.4. Explicit-solvent atomistic MD simulations for the binding study of polymers and peptides

The native conformations of three polymer-binding peptides — HNKSSPLTAALP (PE binder) [29], TSDIKSRSPHHR (PP binder) [30], and HWGMWSY (PS binder) [31] — were obtained by initially constructing linear peptides using the XLEAP module, followed by 100-ns atomistic MD simulations at 300 K in an explicit solvent environment. The peptides were modeled with the Amber 14SB force field [32], and the TIP3P water model was employed for solvation. To assess the progress of peptide folding, the root mean square deviation (RMSD) from the initial conformation was monitored over the entire simulation. Representative equilibrated structures were extracted by performing a *K*-means clustering analysis [33] on the last 5-ns simulation trajectories.

These representative structures of the peptides HNKSSPLTAALP, TSDIKSRSPHHR, and HWGMWSY were then used to simulate peptide binding to their respective polymer. Each polymer-peptide system consisted of six peptide copies and a single polymer particle. For these binding simulations, collapsed chains from 150-mer and 250-mer polymers — previously obtained from polymer folding simulations — were utilized. The PACKMOL package was employed to randomly place the six peptides near the polymer [34]. The resulting polymer–peptide system was solvated in a periodic truncated octahedron with a 1.3 nm buffer of TIP3P water, and neutralized with sodium or chloride counterions. The binding simulations contained four phases: (1) a 1000-step energy minimization using the steepest decent method, with the solvent free to move and the polymer–peptide complex restrained by a harmonic force of 836 $kJ \cdot mol^{-1}$; (2) a 2500-step energy minimization with all atoms free to move; (3) a 50°ps NPT-ensemble MD simulation to heat the system from 0 K to 300 K; and (4) three independent 100-ns production simulations in the canonical (NVT) ensemble to observe peptide binding to the polymer. A 100°ns simulation time was used to ensure system equilibration.

The binding free energy ($\Delta G_{binding}$) of the polymer–peptide complex was calculated on the last 5°ns simulation trajectories, and is defined as [35,36].

$$\Delta G_{binding} = G^{complex} - G^{polymer} - G^{peptide} \quad (1)$$

where $G^{complex}$ represents the free energy of the polymer–peptide complex in solution, and $G^{polymer}$ and $G^{peptide}$ denote the free energies of the polymer and peptide when dissolved separately in solution, respectively. The free energy (G) of a molecule in solution is calculated as:

$$G = \left(U_{int} + U_{vdw} + U_{ele} + G_{egb} + G_{gbsur}\right) - TS_{conf} \quad (2)$$

In this equation, U_{int} is the internal energy related to bond vibrations, bond angles, and dihedral angles. U_{vdw} is the van der Waals energy, calculated using the typical 12-6 Lennard–Jones potentials. U_{ele} is the electrostatic energy, determined by Coulomb's law. G_{egb} is the polar solvation energy, evaluated by the generalized Born method with a variable internal dielectric constant. G_{gbsur} is the non-polar solvation energy, which is proportional to the solvent-accessible surface area of the solute molecule. Finally, TS_{conf} represents configurational entropy, estimated using normal mode analysis.

3. Results and Discussion

3.1. Partial atomic charges and atom types of PE, PP, and PS monomers

Each atom within the PE, PP, and PS monomers was assigned a unique atom name (Fig. 1), where the carbon atoms along all polymer backbones are designated as “C1” and “C2” for clarity. The molecular structures of the PE, PP, and PS monomers were optimized using QM calculations at the HF/6-31G(d) level, while their corresponding ESPs were determined with the B3LYP/6-31G(d) basis set. A two-stage RESP charge-fitting protocol was implemented to fit the computed ESPs into partial atomic charges. The GAFF2 was employed to assign atom types to the PE, PP, and PS monomers, based on their atomic valence states. Fig. 1 presents the optimized molecular configurations, the partial atomic charges, and the atom types for each monomer.

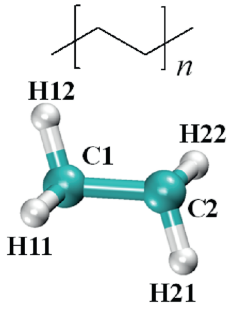
3.2. Simulation studies to examine the validity of GAFF2 force field for the polymer systems

The GAFF2 was developed to accurately describe the thermodynamic properties of biomolecules and organic molecules in the simulations. However, the suitability of the GAFF2 for simulating PE, PP, and PS polymers remains to be evaluated. We calculated the R_g of these polymers in water, along with their densities and C_p in their pure forms. By comparing our simulation results with theoretical predictions and experimental data, we aim to determine whether the GAFF2 is appropriate for modeling the polymers.

***R_g* of polymer chains.** Initial, linear conformations of PE, PP, and PS polymer chains were subjected to implicit-solvent atomistic MD simulations at 500 K for 10 ns, resulting in partially folded structures. These pre-folded polymer chains were then immersed in TIP3P water molecules and underwent an annealing simulation, gradually decreasing from 400 K to 300 K over 100 ns. For each polymer type and chain length, three independent simulation runs were conducted to examine their folding dynamics in explicit solvent conditions. The evolution of polymer configurations over simulation time was monitored by tracking the RMSD of the backbone chains with respect to their respective initial structure from the early implicit solvent runs. Examples that are taken in Fig. S2 refer to the folding states of PE250, PP250, and PS250 during the annealing simulations, illustrating that these polymer chains achieved configurational equilibrium by the end.

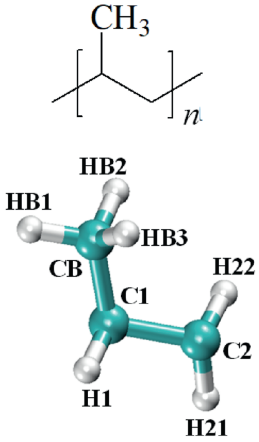
The final equilibrium configurations of the polymer chains in solution are shown in Fig. 2(a). All polymer chains, particularly those with more than 100 monomers, collapsed into a globule form, as expected due to their hydrophobic nature, which causes them to collapse in water. The shape of the collapsed polymers was characterized by R_g, calculated using only the backbone carbon atoms C1 and C2. As shown in Fig. 2(b), the radius of gyration follows a power law relationship, R_g–N^v, where N is the number of monomers. The exponent v obtained from the simulations is 0.342 for PE, 0.324 for PP, and 0.377 for PS. The theoretical scaling law for polymer chains in a collapsed state predicts $v = 0.333$ [37], which is in good agreement with our simulation results. The high

Polyethylene (PE):



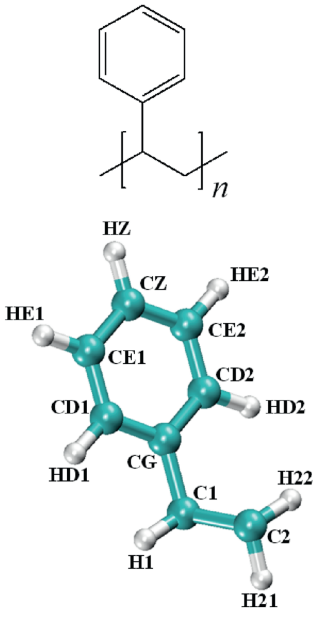
Atom names	Atom types	Partial charges	Atom names	Atom types	Partial charges
C1	c3	0.0396	C2	c3	0.0396
H11	hc	–0.0198	H21	hc	–0.0198
H12	hc	–0.0198	H22	hc	–0.0198

Polypropylene (PP):



Atom names	Atom types	Partial charges	Atom names	Atom types	Partial charges
C1	c3	0.0768	HB3	hc	0.0632
H1	hc	0.0018	C2	c3	–0.0061
CB	c3	–0.2659	H21	hc	0.0019
HB1	hc	0.0632	H22	hc	0.0019
HB2	hc	0.0632			

Polystyrene (PS):



Atom names	Atom types	Partial charges	Atom names	Atom types	Partial charges
C1	c3	0.0004	HZ	ha	0.1248
H1	hc	–0.0053	CE2	ca	–0.0505
CG	ca	0.2509	HE2	ha	0.1058
CD1	ca	–0.2702	CD2	ca	–0.2702
HD1	ha	0.1246	HD2	ha	0.1246
CE1	ca	–0.0505	C2	c3	0.0310
HE1	ha	0.1058	H21	hc	–0.0162
CZ	ca	–0.1888	H22	hc	–0.0162

Fig. 1. Partial atomic charges of PE, PP, and PS monomers, and the corresponding atom types are described using the GAFF2.

coefficient of determination R^2 indicates that R_g is well described by the power law for each polymer type.

Density of pure polymers. Polymer densities were calculated by simulating ten 150-mer polymer chains in the NPT ensemble at 300 K. During the simulation, pressure increased gradually from 10 to 100 kPa in 10 kPa increments. At each pressure step, the system was equilibrated for 5 ns, resulting in a total simulation time of 50 ns. For instance, when examining PE150 polymers, a single simulation indicated that increasing the pressure results in a continuous reduction of the box volume, which in turn causes the

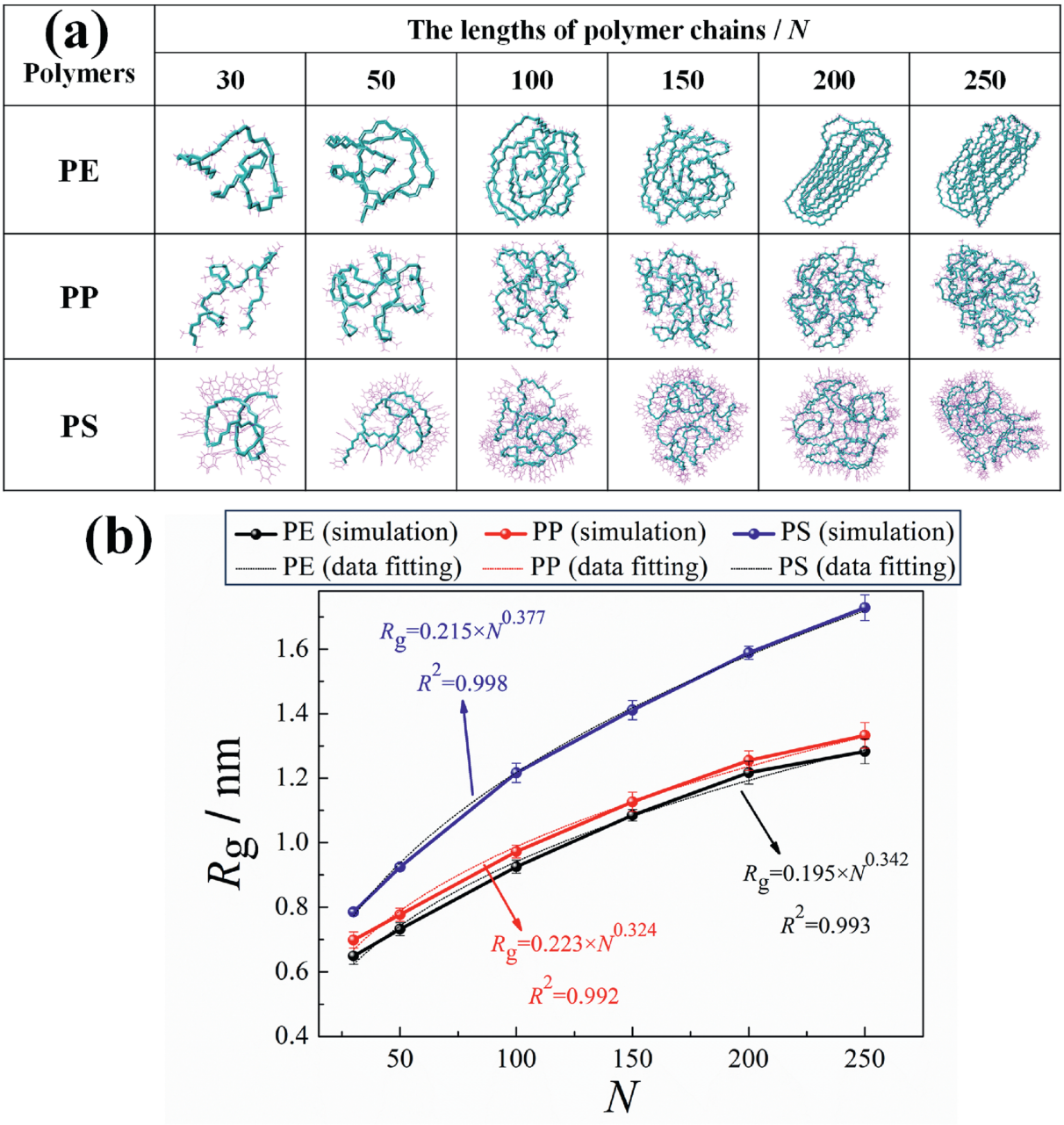
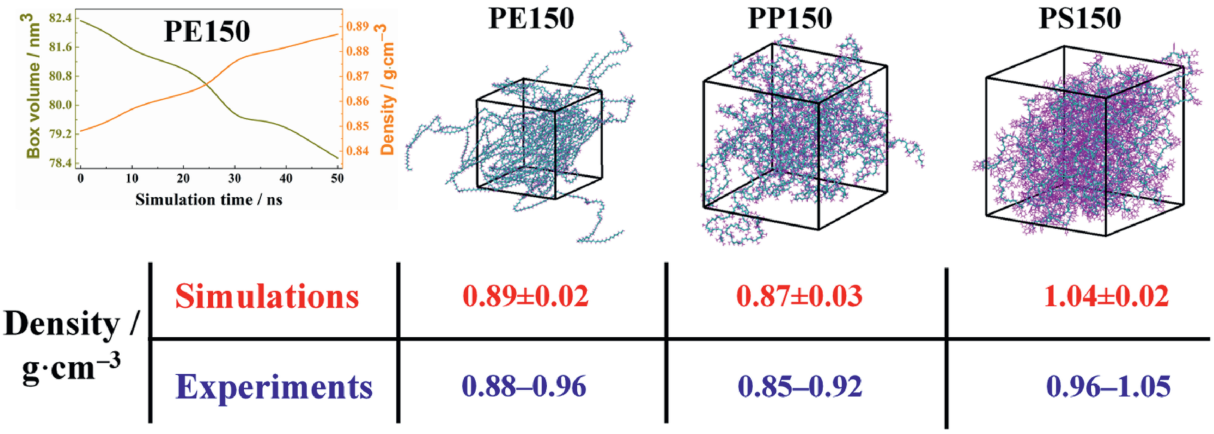


Fig. 2. (a) Equilibrium conformations of PE, PP, and PS with varied chain lengths in 100-ns explicit-solvent atomistic MD simulations. The polymer backbone scaffolds are indicated in cyan color, and the sidechain structures are in purple color. (b) Fitting the simulated radius of gyration (R_g) and the length (N) of the collapsed polymer chains into a power function: R_g–N^v. The simulated scaling exponents v are 0.342 for PE, 0.324 for PP, and 0.377 for PS, which agree with a theoretical scaling law of $v = 0.333$ for the polymers in a collapsed condition.

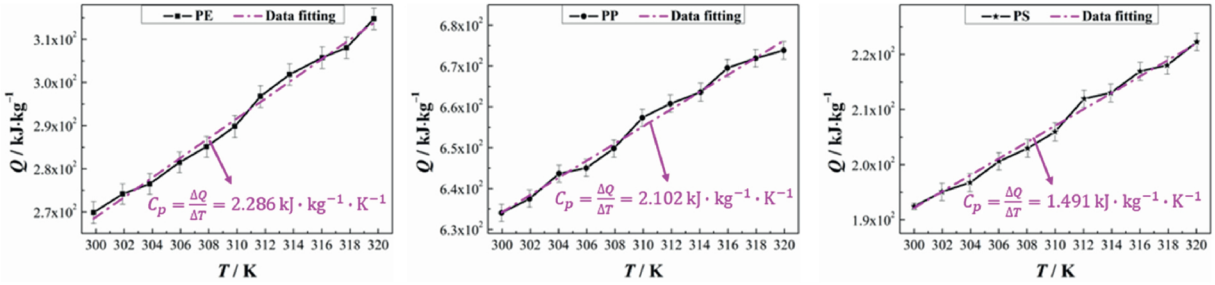
polymer density to increase. At a pressure of 100 kPa, the density of PE was found to be about 0.886 g·cm^{-3}. To minimize potential system deviations, we repeated the simulation protocols four times. The average equilibrium density of polymers was calculated from the volume of the simulation box, yielding values of (0.89 ± 0.02) g·cm^{-3} for PE, (0.87 ± 0.03) g·cm^{-3} for PP, and (1.04 ± 0.02) g·cm^{-3} for PS (Fig. 3). PE exists in both low-density and high-density forms, with densities ranging from 0.88 to 0.96 g·cm^{-3} [38]. The PE system in our simulation appears to represent the low-density form, as its density falls at the lower end of this range. Unlike PE, the experimental densities of PP and PS remain nearly constant at room temperature, with reported values of 0.85–0.92 g·cm^{-3} for PP [39] and 0.96–1.05 g·cm^{-3} for PS [40]. Overall, the simulation results show good agreement with experimental density values for each polymer.

***C*$_p$ of pure polymers.** C_p was determined by performing NPT-ensemble MD simulations on polymer samples. In these simulations, C_p was calculated by measuring the change in enthalpy (ΔQ) over temperature (ΔT), using the equation $C_p = \Delta Q/\Delta T$. Three independent MD simulations were conducted for each system, each containing ten 150-mer polymer chains, at a pressure of 100 kPa and temperatures ranging from 300 to 320 K in 2 K increments. Fitting a straight line to the plots of average enthalpy *versus* temperature gave C_p values: 2.286 kJ·kg^{-1}·K^{-1} for PE, 2.102 kJ·kg^{-1}·K^{-1} for PP, and 1.491 kJ·kg^{-1}·K^{-1} for PS (Fig. 4). For comparison, experimental C_p values sourced from the polymer



Density / g·cm^{-3}	PE150	PP150	PS150
Simulations	0.89±0.02	0.87±0.03	1.04±0.02
Experiments	0.88–0.96	0.85–0.92	0.96–1.05

Fig. 3. MD NPT-ensemble simulations of ten polymer chains of PE150, PP150, and PS150 in a cubic box at 300 K. The computed average densities from four independent simulation runs agree with experimental values.



C_p / kJ·kg^{-1}·K^{-1}	PE	PP	PS
Simulations	2.286	2.102	1.491
Experiments	2.362	1.956	1.358
Deviations	~3.2%	~7.5%	~9.8%

Fig. 4. Plots of enthalpy (Q) *vs.* temperature (T) for the three pure polymers PE150, PP150, and PS150 with ten chains in a cubic box. A linear fitting of the Q–T plots can be used to determine the specific heats (C_p) of the polymers. Comparisons of the computed and experimental C_p values of PE, PP, and PS.

properties database (https://polymerdatabase.com/polymer/physics/HeatCapacity.html) are 2.362 kJ·kg^{-1}·K^{-1} for PE [38], 1.956 kJ·kg^{-1}·K^{-1} for PP [41], and 1.358 kJ·kg^{-1}·K^{-1} for PS [42]. The simulation results for PE show only a slight deviation (~3.2%) from the experimental value, while moderate deviation is observed for PP (~7.5%) and large deviation for PS (~9.8%). Overall, these findings suggest that GAFF2 can predict the heat capacity of polymers with moderate accuracy.

Collectively, the GAFF2 effectively captures the folding behaviors of PE, PP, and PS in aqueous solution, and provides accurate prediction of the pure polymers' densities. While GAFF2 successfully reproduces the C_p of PE, it exhibits moderate errors when predicting the C_p of PP and PS. Therefore, GAFF2 appears to be a reliable choice for atomistic MD simulations of PE, PP, and PS polymers.

3.3. Binding studies of peptides and polymer particles via the MD simulations

Several short peptides were identified using a phage display library for their ability to bind specifically to PE, PP, or PS. The 12-mer sequence HNKSSPLTAALP binds to PE [29], the 12-mer sequence TSDIKSRSPHHR binds to PP [30], and the 7-mer sequence HWGMWSY binds to PS [31]. To gain molecular-level insight into polymer–peptide interactions, explicit-solvent atomistic MD simulations were conducted to investigate the kinetics and thermodynamics of peptide binding to their respective polymers. Each simulation system consisted of six peptide chains, a relaxed 150-mer or 250-mer polymer chain, TIP3P water molecules, and counterions to neutralize the overall charge. Initially, peptides were relaxed in separate simulations and subsequently placed near the polymer using the PACKMOL package, which provided the initial configurations for the peptide–polymer complexes as shown in Figs. 5 and S3. The systems were then simulated at 300 K for 100 ns in three independent runs to reproduce peptide binding events. Six peptides were included to account for binding to different regions of the polymer surface, considering that polymers typically do not possess a specific binding site for peptides. The interfacial contact area (nm^2) between a polymer particle and six adjacent peptides was monitored in the simulation trajectories to examine the dynamics and stability of peptide–polymer interactions during binding. As illustrated in Fig. S4, the association behaviors of three polymer particles (PE250, PP250, and PS250) with their respective peptide sequences — HNKSSPLTAALP, TSDIKSRSPHHR, and HWGMWSY — are demonstrated as the simulations progress. The consistent increase in interfacial contact area reveals that peptide chains are drawn toward the polymer particles through their molecular interactions, thereby resulting in the peptide–polymer binding.

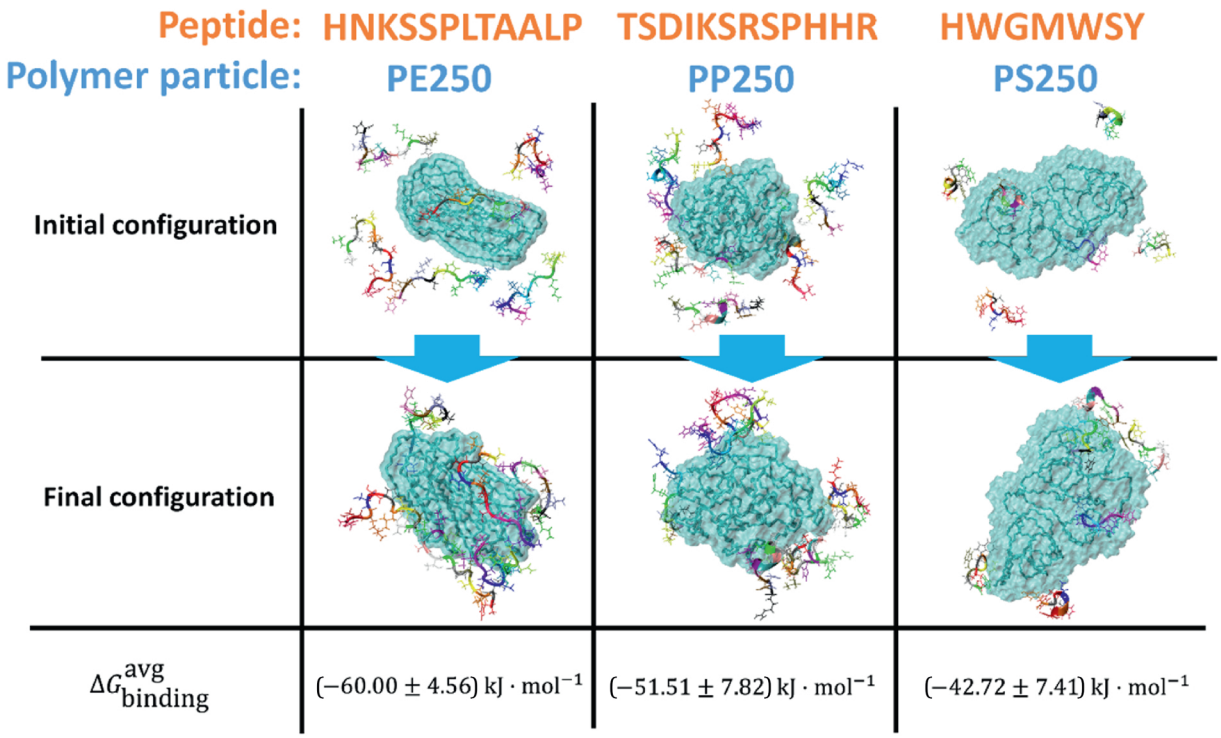


Fig. 5. Explicit-solvent atomistic MD simulations illustrating the binding interactions between peptides and polymer particles. Each simulation setup contains six peptide chains (multi-colored) and a single polymer particle (isosurface) made up of 250 repeating monomers. For each peptide–polymer system, three independent simulation runs are conducted to determine the average binding free energy.

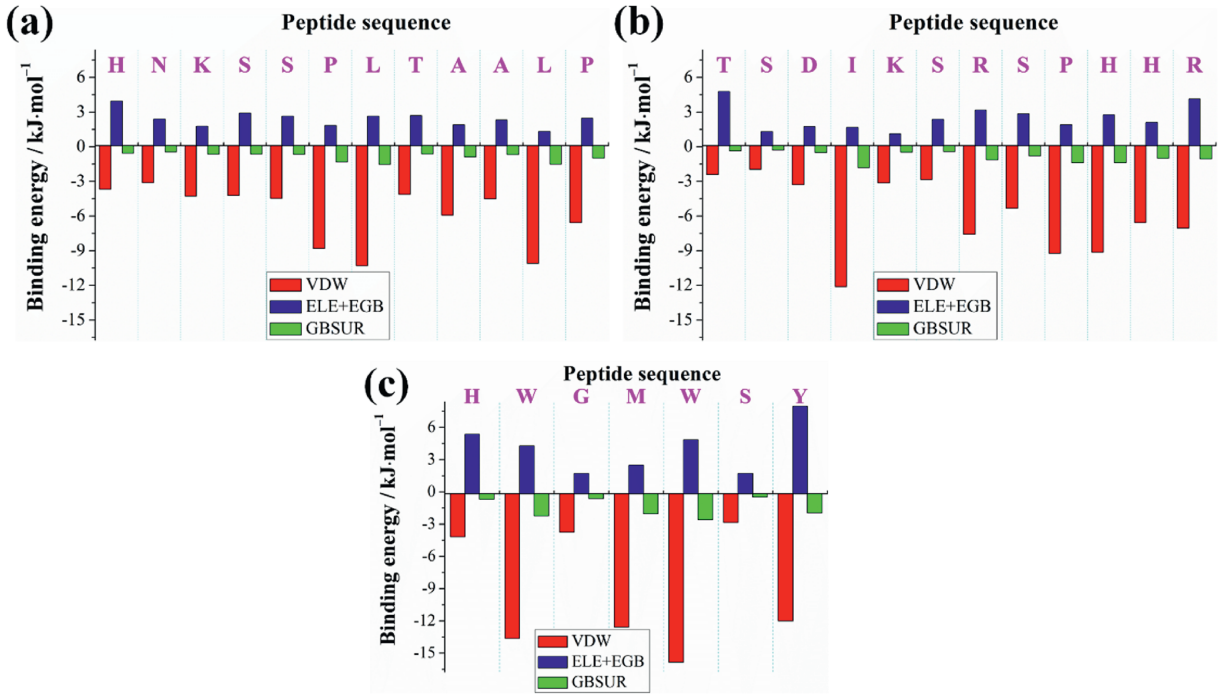


Fig. 6. Energy decompositions of each residue within the three polymer-binding peptides, *viz.* (a) HNKSSPLTAALP, (b) TSDIKSRSPHHR, (c) HWGMWSY, are plotted to analyze their individual VDW, ELE + EGB, and GBSUR contributions to the overall binding energy.

The final configurations of peptide binding simulations using both 250-mer and 150-mer polymer structures are presented in Figs. 5 and S3. Upon comparison, the six peptides appear significantly more crowded on the surface of the 150-mer polymers, which restricts their ability to extend their chain conformations (Fig. S3). In contrast, the 250-mer polymers provide a greater surface area, making them a more suitable choice for binding simulations involving multiple peptides. The average binding free

energies ($\Delta G^{avg}_{binding}$) of each peptide and polymer particle were calculated over the last 5-ns simulation trajectories (Fig. 5). The large, negative binding free energies observed for each peptide indicates strong binding affinity to their respective polymers, which agree well with the experimental observations.

Herein, an additional reference MD simulation was performed for a mismatched system that included six HNKSSPLTAALP chains and a single PS250 particle to assess the peptide's selectivity for a particular polymer (Fig. S5). Our simulation demonstrated that only two out of the six peptide chains interact with the PS250 particle, indicating that HNKSSPLTAALP peptides no longer show specific affinity for PS. The GAFF2 effectively models the molecular recognition between peptides and polymers.

Decomposition of the binding energy into VDW energy, electrostatic and polar solvent energies (ELE + EGB), and non-polar contributions (GBSUR) allows for a detailed understanding of the significance of each residue and interaction types in peptide binding. Fig. 6 illustrates these energy contributions for the three peptides. VDW interactions are strongly negative, favoring binding, whereas the charge-charge (ELE + EGB) energies are positive, thereby impeding binding. GBSUR energy has a small negative value for each residue. Recalling that GBSUR is determined by the surface area exposed to solvent, this suggests that the residues are buried within the polymer surface than exposed to the water.

Further insight into peptide binding can be gained by analyzing the composition of each peptide. The PE-binding peptide, HNKSSPLTAALP, contains six hydrophobic and six polar residues. The hydrophobic residues consistently provide the most significant contributions to PE binding through VDW interactions, especially the proline (P) at sites 6 and 12, and leucine (L) at sites 7 and 11. The PP-binding peptide, TSDIKSRSPHHR, is relatively hydrophilic, with only two hydrophobic residues: isoleucine (I) at site 4 and proline (P) at site 9. These hydrophobic residues strongly influence binding, while notable contributions also come from the positively charged arginine (R) at sites 7 and 12, and the polar histidine (H) at sites 10 and 12. The PS-binding peptide, HWGMWSY, features four hydrophobic residues — tryptophan (W) at sites 2 and 5, methionine (M) at site 4, and tyrosine (Y) at site 7 — all of which contribute to PS binding *via* VDW interactions. The remaining three polar residues make comparatively weaker contributions to peptide binding.

4. Conclusions

Polymer–peptide interactions are crucial for functionalizing smart materials across a range of bio-applications, such as the development of peptide-functionalized particle cleaners designed to capture and recover microplastics and nanoplastics from the environment. Atomistic MD simulations serve as powerful computational tools that provide insights into the microscale interactions between polymers and peptides, which are often inaccessible through experimental techniques.

In this study, QM calculations were first conducted to determine the partial atomic charges of the monomers in PE, PP, and PS by following a two-stage RESP charge-fitting protocol. To validate the suitability of the GAFF2 for these polymers, we performed atomistic MD simulations to examine the folded conformations of PE, PP, and PS chains of varying lengths in solution. The radius of gyration of the polymer chains was evaluated as a function of the chain length N, satisfying the theoretical prediction of $R_g - N^v$ with $v = 0.333$ for collapsed states. Additionally, we computed the densities and C_p of the pure polymers in the MD simulations and compared these results to experimental measurements. It turned out that the computed densities for PE, PP and PS accord well with the experimental values. While the predicted C_p for PE was highly accurate, the C_p values for PP and PS showed minor deviations from experimental data. Overall, the GAFF2 proves to be reliable for polymer simulations, although minor deficiencies remain.

Three short phage-discovered peptides — HNKSSPLTAALP, TSDIKSRSPHHR, and HWGMWSY — were studied in explicit-solvent atomistic MD simulations for their binding affinities to PE, PP, and PS, respectively. In each binding simulation, six relaxed peptide chains and a single polymer particle were included. The simulation results demonstrated that HNKSSPLTAALP exhibited the strongest affinity to the PE particle, with an average binding free energy $\Delta G^{avg}_{binding} = -60.00\ kJ\cdot mol^{-1}$. This was followed by TSDIKSRSPHHR binding to the PP particle with an affinity of $\Delta G^{avg}_{binding} = -51.51\ kJ\cdot mol^{-1}$, and HWGMWSY binding to the PS particle with an affinity of $\Delta G^{avg}_{binding} = -42.72\ kJ\cdot mol^{-1}$. All three peptides were confirmed by MD simulations to be effective binders for their respective polymers. Additionally, the binding energies of each polymer–peptide complex were decomposed along the peptide sequences to assess the contribution of individual residues to the overall association with the polymer particles. This analysis identified several key residues, which primarily contribute VDW interactions responsible for binding to the polymers.

CRediT Authorship Contribution Statement

Yingqian Ren: Writing – original draft, Visualization, Validation, Formal analysis, Data curation. Mingyu Wang: Writing – original draft, Validation, Data curation. Jipeng Li: Writing – original draft, Supervision, Conceptualization. Xingqing Xiao: Writing – review & editing, Writing – original draft, Supervision, Methodology, Conceptualization.

Declaration of Competing Interest

The authors declare that they have no known competing financial interests or personal relationships that could have appeared to influence the work reported in this paper.

Acknowledgements

This research was supported by funds from the National Natural Science Foundation of China (22268016 and 22566018), the Hainan Provincial Natural Science Foundation of China (425RC691) and the Research Start-Up Grant Program of Hainan University (KYQD(ZR)-21157). We also thank the High-Performance Computing Center of Hainan University for providing computing resources.

Supplementary Material

Supplementary data to this article can be found online at https://doi.org/10.1016/j.cjche.2026.01.026.

References

[1] D. Gola, P.K. Tyagi, A. Arya, N. Chauhan, M. Agarwal, S.K. Singh, S. Gola, The impact of microplastics on marine environment: A review, *Environ. Nanotechnol. Monit. Manag.* 16 (2021) 100552.
[2] A. Akbari, J. Jaafari, Entry pathway and potential impacts of microplastics in air, water, soil and human health: A review, *Casp. J. Health Res* 9 (4) (2024) 181–198.
[3] K. Pabortsava, R.S. Lampitt, High concentrations of plastic hidden beneath the surface of the Atlantic Ocean, *Nat. Commun.* 11 (2020) 4073.
[4] S. Wagner, T. Reemtsma, Things we know and don't know about nanoplastic in the environment, *Nat. Nanotechnol.* 14 (4) (2019) 300–301.

[5] A.D. Vethaak, J. Legler, Microplastics and human health, *Science* 371 (6530) (2021) 672–674.
[6] C.N. Loney, S. Maheshwari, N. Pramounmat, M.J. Janik, J.N. Renner, Effects of peptide-functionalized surfaces on the electrochemical hydrogen evolution reaction, *J. Electrochem. Energy Convers. Storage* 17 (4) (2020) 040801.
[7] L.L. Zhu, H.Y. Zhao, Z.Y. Zhou, Y.H. Xia, Z.G. Wang, H.T. Ran, P. Li, J.L. Ren, Peptide-functionalized phase-transformation nanoparticles for low intensity focused ultrasound-assisted tumor imaging and therapy, *Nano Lett.* 18 (3) (2018) 1831–1841.
[8] T. Sawada, M. Takizawa, T. Serizawa, Affinity-based functionalization of biomedically utilized micelles composed of triblock copolymers through polymer-binding peptides, *ACS Biomater. Sci. Eng.* 5 (11) (2019) 5714–5720.
[9] T. Sawada, S. Suzuki, T. Serizawa, Affinity-based thermoresponsive fluorescence switching of proteins conjugated with a polymer-binding peptide, *Soft Matter* 16 (44) (2020) 10096–10100.
[10] R. Derda, S.K.Y. Tang, S.C. Li, S. Ng, W. Matochko, M.R. Jafari, Diversity of phage-displayed libraries of peptides during panning and amplification, *Molecules* 16 (2) (2011) 1776–1803.
[11] X.Q. Xiao, P.F. Agris, C.K. Hall, Designing peptide sequences in flexible chain conformations to bind RNA: A search algorithm combining Monte Carlo, self-consistent mean field and concerted rotation techniques, *J. Chem. Theor. Comput.* 11 (2) (2015) 740–752.
[12] X.Q. Xiao, P.F. Agris, C.K. Hall, Introducing folding stability into the score function for computational design of RNA-binding peptides boosts the probability of success, *Proteins* 84 (5) (2016) 700–711.
[13] X.Q. Xiao, M.E. Hung, J.N. Leonard, C.K. Hall, Adding energy minimization strategy to peptide-design algorithm enables better search for RNA-binding peptides: redesigned λ N peptide binds *boxB* RNA, *J. Comput. Chem.* 37 (27) (2016) 2423–2435.
[14] X.Q. Xiao, Y.M. Wang, J.N. Leonard, C.K. Hall, Extended concerted rotation technique enhances the sampling efficiency of the computational peptide-design algorithm, *J. Chem. Theor. Comput.* 13 (11) (2017) 5709–5720.
[15] D.A. Grela, V. Zannoni, N.M. Vizioli, Studying the interaction between peptides and polymeric nanoparticles used as pseudostationary phase in capillary electrochromatography, *Microchem. J.* 130 (2017) 153–156.
[16] E. Adediran, S. Vijayanand, A. Kale, M. Gulani, J.C. Wong, A. Escayg, K.S. Murnane, M.J. D'Souza, Microfluidics-assisted formulation of polymeric oxytocin nanoparticles for targeted brain delivery, *Pharmaceutics* 17 (4) (2025) 452.
[17] D.H. Cho, J.I. Hahm, Protein–polymer interaction characteristics unique to nanoscale interfaces: A perspective on recent insights, *J. Phys. Chem. B* 125 (23) (2021) 6040–6057.
[18] A. Maslovskis, J.B. Guilbaud, I. Grillo, N. Hodson, A.F. Miller, A. Saiani, Self-assembling peptide/thermoresponsive polymer composite hydrogels: Effect of peptide–polymer interactions on hydrogel properties, *Langmuir* 30 (34) (2014) 10471–10480.
[19] R.V. Ulijn, A. Lampel, Order/disorder in protein and peptide-based biomaterials, *Isr. J. Chem.* 60 (12) (2020) 1129–1140.
[20] P.A. Taylor, A. Jayaraman, Molecular modeling and simulations of peptide–polymer conjugates, *Annu. Rev. Chem. Biomol. Eng.* 11 (2020) 257–276.
[21] S.L. Baker, A. Munasinghe, H. Murata, P. Lin, K. Matyjaszewski, C.M. Colina, A. J. Russell, Intramolecular interactions of conjugated polymers mimic molecular chaperones to stabilize protein–polymer conjugates, *Biomacromolecules* 19 (9) (2018) 3798–3813.
[22] O. Bertran, D. Curcó, D. Zanuy, C. Alemán, Atomistic organization and characterization of tube-like assemblies comprising peptide–polymer conjugates: computer simulation studies, *Faraday Discuss* 166 (2013) 59–82.
[23] G. Collier, N.A. Vellore, J.A. Yancey, S.J. Stuart, R.A. Latour, Comparison between empirical protein force fields for the simulation of the adsorption behavior of structured LK peptides on functionalized surfaces, *Biointerphases* 7 (1–4) (2012) 24.
[24] D. Vassetti, M. Pagliai, P. Procacci, Assessment of GAFF2 and OPLS-AA general force fields in combination with the water models TIP3P, SPCE, and OPC3 for the solvation free energy of druglike organic molecules, *J. Chem. Theor. Comput.* 15 (3) (2019) 1983–1995.
[25] Z.X. Sun, P. Procacci, Methodological and force field effects in the molecular dynamics-based prediction of binding free energies of host–guest systems, *Phys. Chem. Chem. Phys.* 26 (29) (2024) 19887–19899.
[26] S. Zhu, Validation of the generalized force fields GAFF, CGenFF, OPLS-AA, and PRODRGFF by testing against experimental osmotic coefficient data for small drug-like molecules, *J. Chem. Inf. Model.* 59 (10) (2019) 4239–4247.
[27] P. Cieplak, W.D. Cornell, C. Bayly, P.A. Kollman, Application of the multimolecule and multiconformational RESP methodology to biopolymers: Charge derivation for DNA, RNA, and proteins, *J. Comput. Chem.* 16 (11) (1995) 1357–1377.
[28] R. Bhowmik, S. Sihn, V. Varshney, A.K. Roy, J.P. Vernon, Calculation of specific heat of polymers using molecular dynamics simulations, *Polymer* 167 (2019) 176–181.
[29] S.D. Cunningham, D.J. Lowe, J.P. O'Brien, H. Wang, A.E. Wilkins, Polyethylene binding peptides and methods of use, US Pat., 7906617B2, 2011.
[30] S.D. Cunningham, D.J. Lowe, J.P. O'Brien, H. Wang, A.E. Wilkins, Polypropylene binding peptides and methods of use, US Pat., 7928076B2, 2011.
[31] M. Vodnik, B. Strukelj, M. Lunder, HWGMWSY, an unanticipated polystyrene binding peptide from random phage display libraries, *Anal. Biochem.* 424 (2) (2012) 83–86.
[32] J.A. Maier, C. Martinez, K. Kasavajhala, L. Wickstrom, K.E. Hauser, C. Simmerling, ff14SB: improving the accuracy of protein side chain and backbone parameters from ff99SB, *J. Chem. Theor. Comput.* 11 (8) (2015) 3696–3713.
[33] L.X. Chen, D.R. Roe, M. Kochert, C. Simmerling, R.A. Miranda-Quintana, K-means NANI: An improved clustering algorithm for molecular dynamics simulations, *J. Chem. Theor. Comput.* 20 (13) (2024) 5583–5597.
[34] L. Martínez, R. Andrade, E.G. Birgin, J.M. Martínez, PACKMOL: A package for building initial configurations for molecular dynamics simulations, *J. Comput. Chem.* 30 (13) (2009) 2157–2164.
[35] H. Gohlke, C. Kiel, D.A. Case, Insights into protein–protein binding by binding free energy calculation and free energy decomposition for the ras–raf and ras–RalGDS complexes, *J. Mol. Biol.* 330 (4) (2003) 891–913.
[36] X.Q. Xiao, B.W. Zhao, P.F. Agris, C.K. Hall, Simulation study of the ability of a computationally-designed peptide to recognize target tRNA(Lys 3) and other decoy tRNAs, *Protein Sci.* 25 (12) (2016) 2243–2255.
[37] A. Rey, J.J. Freire, M. Bishop, J.H.R. Clarke, Radius of gyration and viscosity of linear and star polymers in different regimes, *Macromolecules* 25 (4) (1992) 1311–1315.
[38] B. Wunderlich, Motion in polyethylene. I. Temperature and crystallinity dependence of the specific heat, *J. Chem. Phys.* 37 (6) (1962) 1203–1207.
[39] C. De Rosa, F. Auriemma, P. Corradini, O. Tarallo, S. Dello Iacono, E. Ciaccia, L. Resconi, Crystal structure of the trigonal form of isotactic polypropylene as an example of density-driven polymer structure, *J. Am. Chem. Soc.* 128 (1) (2006) 80–81.
[40] U. Gaur, B. Wunderlich, Heat capacity and other thermodynamic properties of linear macromolecules. V. Polystyrene, *J. Phys. Chem. Ref. Data* 11 (2) (1982) 313–325.
[41] E. Passaglia, H.K. Kevorkian, Specific heat of atactic and isotactic polypropylene and the entropy of the glass, *J. Appl. Phys.* 34 (1) (1963) 90–97.
[42] R.W. Warfield, M.C. Petree, Thermodynamic properties of polystyrene and styrene, *J. Polym. Sci.* 55 (162) (1961) 497–505.